Rupture complexity of a moderate intraplate earthquake in the Alps: the 1996M5 Epagny–Annecy earthquake

F. Courboulex, N. Deichmann, J.-C. Gariel

Geophys. J. Int. (1999) **139,** 152–160

Rupture complexity of a moderate intraplate earthquake in the Alps: the 1996 *M*5 Epagny–Annecy earthquake

Françoise Courboulex,[1] Nicholas Deichmann[2] and Jean-Christophe Gariel[3]

[1] *UMR Géosciences Azur, UNSA, CNRS,* 06560 *Valbonne, France. E-mail: courboul@faille.unice.fr*
[2] *Swiss Seismological Service, ETH-Hönggerberg,* 8093 *Zürich, Switzerland*
[3] *Institut de Protection et de Sureté nucléaire,* 92265 *Fontenay aux Roses, France*

Accepted 1999 May 21. Received 1999 May 17; in original form 1998 November 20

SUMMARY

The magnitude 5 Epagny–Annecy earthquake of 1996 July 15 is the largest seismic event to have occurred in the Alps since the introduction of modern digital instrumentation. This strike-slip event was located on the Vuache Fault, near the town of Annecy, in the northern French Alps.

The aim of our work was to retrieve the main parameters of the rupture process of this earthquake from seismograms recorded at local and regional distances (20–300 km). To eliminate path and site effects from the seismograms, we compared the main shock recordings at each station with those of the largest aftershocks nearby. We used a combination of techniques, including pulse-width measurements and cross-correlation of velocity traces, comparison of *P*-wave displacement pulses, and empirical Green's function deconvolution, to retrieve the apparent duration of the rupture process as seen at each station. Our results demonstrate that, in the absence of on-scale data, *P*-wave pulse-width measurements on clipped signals can be misleading if the rupture process is complex. In the case of the Annecy earthquake, comparisons of on-scale *P*-wave displacement seismograms and the empirical Green's function deconvolutions show that the rupture process consisted of at least two subevents separated by 0.2–0.3 s, and with a total duration of about 0.5 s. The systematic azimuthal dependence of both the shape and duration of the apparent source-time function is consistent with a nearly unilateral propagation of the main rupture phase in a southeast direction along the fault plane and parallel to the direction of slip. An isochron analysis reveals that the first subevent occurred slightly to the northwest of the nucleation point but that the second subevent was located further to the southeast, thus confirming the overall rupture directivity towards the southeast. An interpretation of our results in light of the previously documented aftershock distribution and of observations of ground cracks in the epicentral area suggests that the main shock occurred on the Vuache Fault, and that rupture in a northwest direction was inhibited by a right-lateral stepover in the fault. Accordingly, the vast majority of the subsequent aftershocks, which include several magnitude 3–4 events, occurred on a fault segment that is slightly offset from the inferred surface trace of the Vuache Fault and that was activated by the main shock.

Key words: Alps, earthquake-source mechanism, Green's function, intraplate, rupture.

INTRODUCTION

Most seismic source studies have been undertaken for earthquakes with magnitudes larger than 6. The reason for this is not only the social impact of such large events, but also the need for there to be enough records of the required quality. Recently, with the development of dense seismic networks, more and more seismologists have tried to study the rupture process of moderate and small earthquakes (Hough 1996; Beroza & Ellsworth 1996; Mori 1996; Courboulex *et al.* 1996; Haddon & Adams 1997; Courboulex *et al.* 1998; Fletcher & Spudich 1998). However, these studies are still rare because of the lack or the low quality of near-source data and because of difficulties in the interpretation of the results. In regions such as central Europe, where no large earthquakes have been recorded, it is especially important to study in detail the rupture processes of moderate-size events, since they are the only witness of rapid movement on active faults.

In this paper we study the source process of the Epagny–Annecy earthquake of 1996. This event, which occurred on 1996 July 15 at 00 : 13 near the city of Annecy, in the northern part of the French Alps, reached an epicentral intensity of VII–VIII (MSK) and caused total damages to buildings estimated at 300 million French francs (about 50 million US dollars). Magnitude estimates range between 4.2 and 5.3 with a median value of 5.0 (Thouvenot *et al.* 1998). A comprehensive paper by Thouvenot *et al.* (1998) presents the main-shock and the aftershock locations and focal solutions, as well as details of the seismotectonic setting, site effects and other coseismic phenomena.

For our purpose, the Epagny–Annecy event is of particular interest for several reasons:

(1) it is the most significant earthquake to have occurred in the Alps since the beginning of digital instrumental observations (Vogt 1979; Nicolas *et al.* 1990; Lambert & Levret-Albaret 1996) and has been recorded by many stations at local and regional distances in France, Italy and Switzerland;

(2) it was followed by several hundreds of aftershocks which were also recorded by local and regional seismic networks;

(3) it is clearly related to a well-known strike-slip fault that reaches the surface (the NW–SE-trending Vuache fault), as demonstrated by the focal mechanism (Fig. 1), the aftershock locations (Fig. 9) and the shallow focal depth of 2–3 km (Thouvenot *et al.* 1998).

The aim of this study is to retrieve the source dimension, the duration of the rupture process, its directivity and its relation to the aftershock distribution. Using all the available recordings of the main shock and the largest aftershocks, we adopted an empirical Green's function approach to remove the contributions of path and instrument from the seismograms of the main shock.

AVAILABLE DATA

The Epagny–Annecy earthquake was recorded by many seismic networks in France (LDG[1], IPSN[2], Sismalp[3], Renass[4], TGRS[5], Rosalp[6], RAP[7]), in Italy (Dister[8]) and in Switzerland (SED[9]).

We made a selection among this large number of records: first, we kept only the stations that recorded both the main shock and at least one of the largest aftershocks that was suitable as an empirical Green's function; second, we selected the seismograms that were recorded at a sampling frequency higher than 60 Hz, in order to be able to work on small events (magnitude 3–4). This left us with 36 stations that provided either local seismograms with a *Pg* wave as first arrival or regional seismograms with a *Pn* wave as first arrival. From these stations, 16 records were clipped because of insufficient dynamic range and 20 were on-scale. We decided to analyse clipped and unclipped seismograms separately in order to check whether these two types of data give the same results. The final set of stations used is shown in Fig. 1, with different symbols depending on whether the main shock records were clipped or not.

[1] Laboratoire de Géophysique du Commisariat à l'énergie atomique.
[2] Institut de Protection et de Sureté Nucléaire.
[3] Dense short-period network operated by the Observatory of Grenoble.
[4] Réseau National de surveillance sismique.
[5] Broad-band network operated by the UMR Géosciences Azur.
[6] Broad-band network operated by Observatory of Grenoble.
[7] Réseau Accélérométrique permanent Français.
[8] Dipartimento di Scienze della Terra, Genova.
[9] Swiss Seismological Service.

DATA ANALYSIS

One difficulty in seismic source studies is the removal of path and site effects from the observed seismograms. In the case of the Annecy earthquake, this removal is not easy because the crustal structure in the Alps is complex and not well known and because the source was shallow (2–3 km), causing the ray paths to be strongly affected by the near-surface layers. At the relatively high frequencies of interest here, it is therefore impossible to compute theoretical Green's functions with sufficient accuracy. A common approach to circumventing this problem is to use the seismograms of a smaller event as an empirical Green's function (EGF) (Hartzell 1978; Mueller 1985). The conditions for this technique to work are that the source of the smaller event is located close enough to the hypocentre of the main shock and that it has a similar focal mechanism. Moreover, the small event must be sufficiently

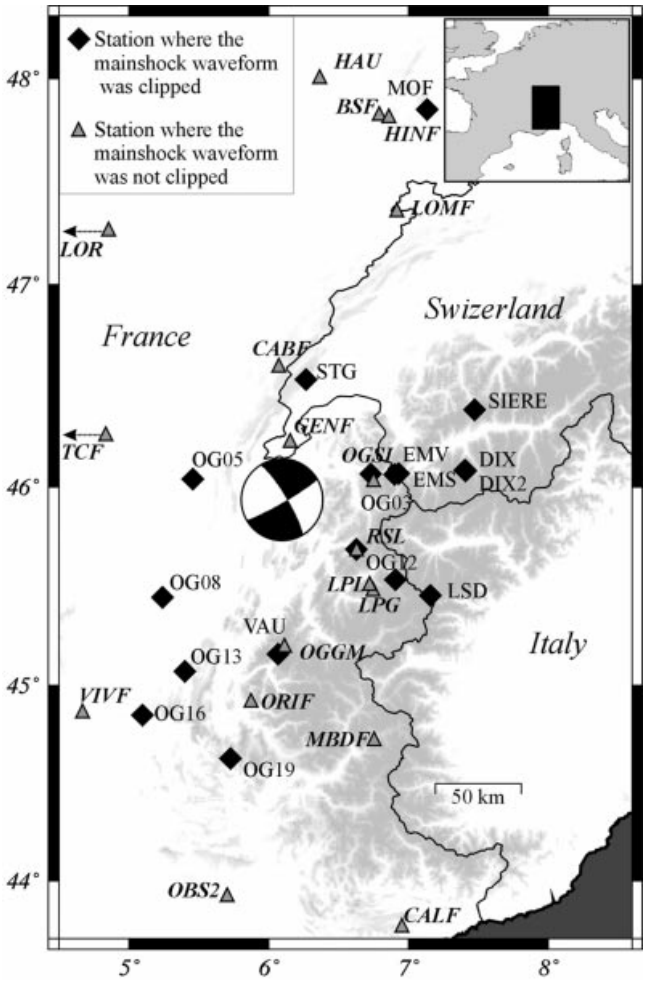

Figure 1. Focal mechanism of the 1996 July 15 Epagny–Annecy event from Thouvenot *et al.* (1998) and stations that were used in this study. Black diamonds represent those stations at which the records of the main shock are clipped, whereas grey triangles correspond to those stations from which unclipped records are available.

small that the duration of its source-time function (STF) is short enough to be negligible compared with that of the main shock while still being strong enough to provide records with good signal-to-noise ratios at a large number of stations. In our case, we chose as EGFs two aftershocks with magnitudes M_L (estimated by Renass) equal to 3.7 and 3.4. The first one occurred about 5 hr after the main shock and was located almost at the same point (Thouvenot *et al.* 1998). The second one, which occurred 5 days later (1996 July 20 22:04), was located 1.5 km to the northwest, at a slightly shallower depth than the main shock. Both events have a strike-slip focal mechanism very similar to the one of the main shock (difference in strike $<14°$, difference in dip $<10°$; F. Thouvenot, personal communication).

The deconvolution of the main shock by the EGF results in an apparent relative source-time function (ARSTF). This ARSTF represents the temporal history of the moment release at the source as seen from a given station. It is 'apparent' because the shape of the source-time function depends on the direction from which the rupture propagation is viewed, and it is 'relative' because it is scaled by the moment of the EGF and its duration is reduced by the source duration of the EGF. We performed the deconvolution in the time domain using a non-linear deconvolution method with positivity constraint (Courboulex *et al.* 1996) on the two EGFs separately. The use of more than a single event as EGF is very important in such an analysis to confirm the reliability of the results.

Waveform comparison and EGF deconvolution

Before performing the EGF deconvolutions, we systematically compared the waveforms of the main shock and the aftershocks at each station that provided unclipped records. It is important to note that we used only *P* waves, because the *S* waves were very complex and could not be identified clearly. This may be a result of the shallow depth of the hypocentres, which leads to the generation of strong surface waves that reach the station at almost the same time as the *S* waves.

At many stations, the main shock and the aftershock waveforms are similar, and the *P*-wave arrivals have a simple shape (e.g. station RSL in Fig. 2). At other stations, both the displacement and the velocity traces of the main shock feature a double-pulse *P*-wave onset, which is not seen in the seismograms of the aftershocks (e.g. station CABF in Fig. 2). Moreover, in all cases showing signs of a double-pulse *P*-wave onset, cross-correlations of the main shock velocity signals with those of the aftershocks result in a maximum of the correlation coefficient when the aftershock is shifted by almost 0.3 s relative to the observed first breaks ($\delta\tau$ in Fig. 2). Shifted in this way, the *P*-wave onset of the aftershock is aligned with the second pulse of the main shock. This is because the second pulse is in general larger and longer than the first one and thus dominates the later stages of the seismograms.

The results of the EGF deconvolutions confirm that the double pulse is a feature of the STF of the main shock, but that it is not seen at all azimuths (see Fig. 2). Indeed, the double-pulse ARSTFs with a relatively long overall duration are observed only at stations situated north of the epicentre, while at all other stations the ARSTFs are simpler and shorter (Fig. 3). The durations of the apparent source-time function measured directly on the displacement pulse, and on the result of EGF deconvolution are reported in Table 1.

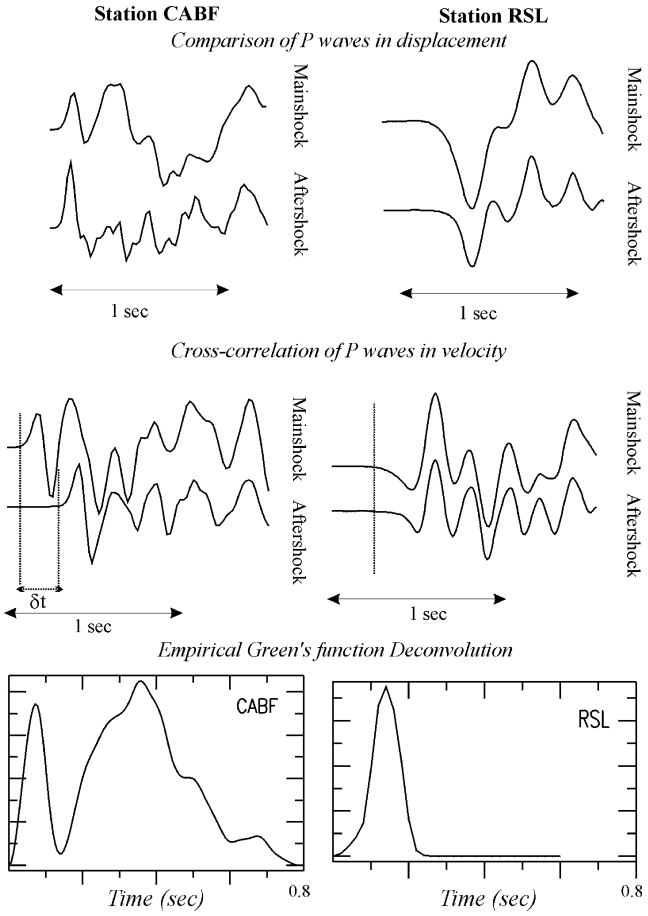

Figure 2. Examples of displacement and velocity waveforms of the main shock compared with those of the aftershock of 1996 July 15 05:46, and results of the EGF deconvolution at stations located north (CABF) and southeast (RSL) of the epicentre. The displacement traces at RSL were corrected for the response of the 1 Hz seismometer before integration.

It is clear that such behaviour is not compatible with a symmetric or bilateral rupture expansion. Based on the fact that the fault plane strikes in the direction of the Vuache Fault (Thouvenot *et al.* 1998), and that all the double-pulse long-duration STFs are observed at stations north of the epicentre, we expect that the rupture consisted of at least two subevents and propagated preferentially towards the southeast.

Pulse-width measurements

As first demonstrated by O'Neill & Healy (1973), an alternative method of obtaining information about the duration of the STF consists of measuring the width of the first half-cycle of the *P*-wave onset as recorded by a standard seismometer sensitive to ground velocity. This method is simple and has the advantage of being applicable also to severely clipped seismograms. The observed pulse width is a function of the rise time of the STF, modified by broadening due to the response of the recording instrument as well as to attenuation and scattering along the path. In a first approximation, the path and instrument contributions to the pulse widths at each station can be corrected by subtracting the pulse width of a smaller event (Frankel & Kanamori 1983). Provided that possible directivity effects of the

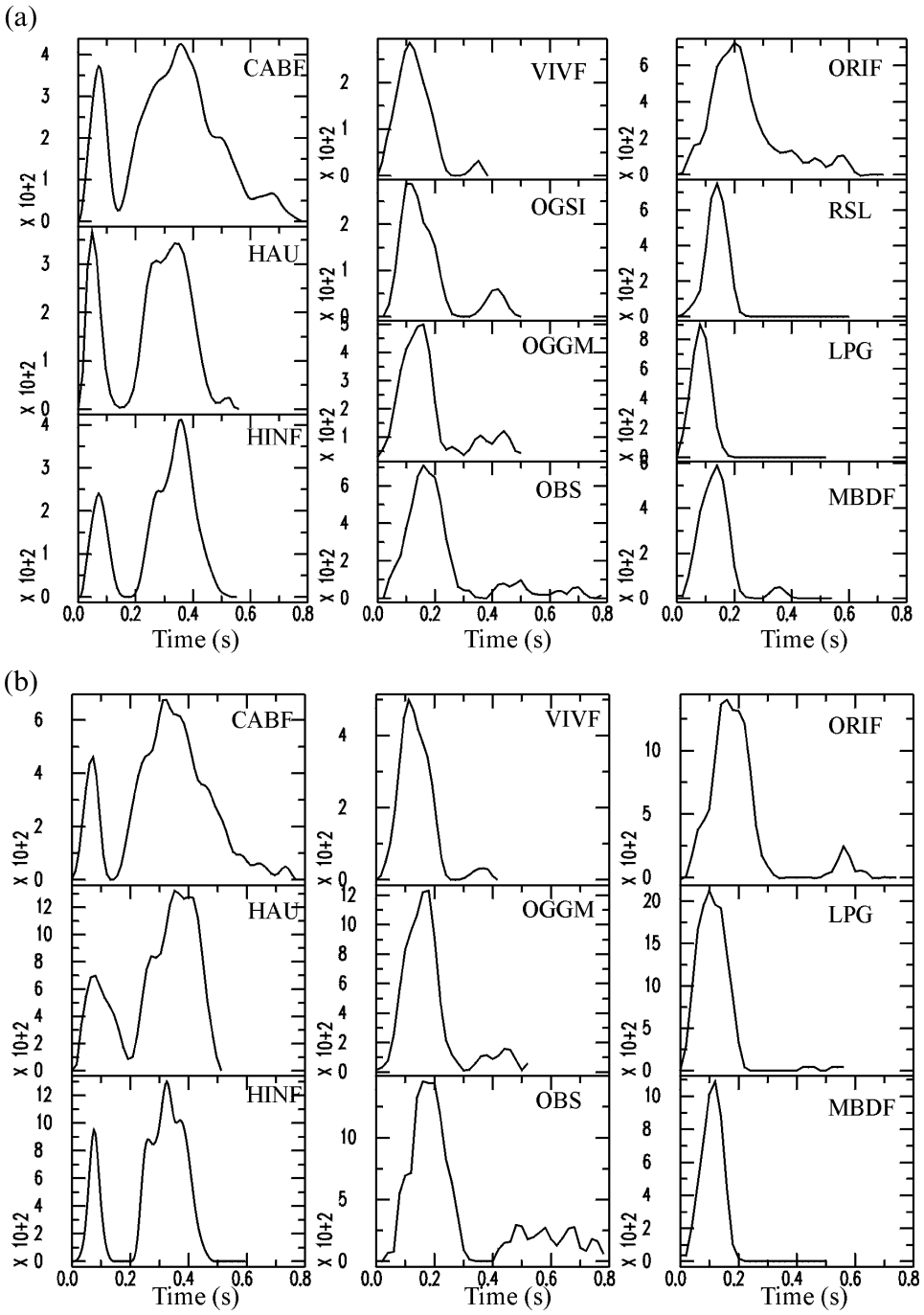

Figure 3. Deconvolution results with: (a) the $M_L = 3.7$ and (b) the $M_L = 3.4$ aftershock as EGF.

smaller event's rupture process are negligible, this technique will in general give a reliable measure of azimuthal variations in the apparent duration of the main shock STF.

As illustrated by the example shown in Fig. 4, the relative pulse widths measured from clipped seismograms at all stations situated north of the epicentre are consistently smaller than those observed at stations south of the epicentre. From pulse-width measurements on clipped records alone we would thus conclude that, contrary to the results of the EGF deconvolutions, the rupture propagated towards the northwest. Obviously, the reason for this discrepancy is that on the clipped records we cannot recognize the fact that towards the north the STF of the main shock appears as a double pulse and that at the northern stations we have therefore measured only the relative duration of the first pulse. This shows that, in the presence of undetected rupture complexities, a naive application of the pulse-width method can produce severely misleading results.

INTERPRETATION

Unilateral rupture model

To visualize the distribution of the double- and single-pulse source-time functions relative to the focal mechanism, we

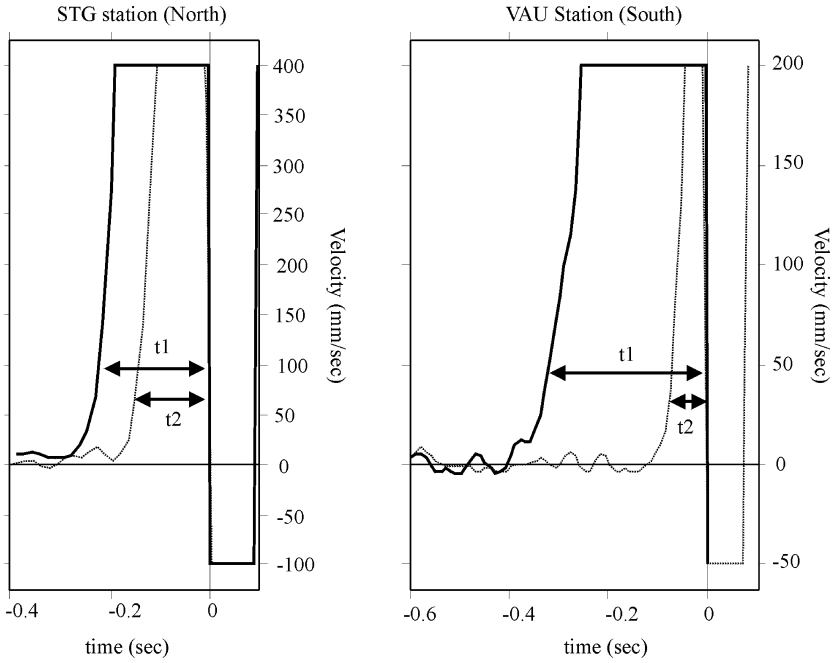

Figure 4. Examples of two pulse-width measurements on clipped seismograms.

Table 1. *P*-pulse duration and apparent relative STF duration for each station that recorded the main shock without saturation. 'u' indicates that the value was undefined.

station name	network	epicentral distance (km)	azimuth (°)	*P* pulse duration (s)	ARSTF duration (s)
OGSI	RAP	48	78	0.3	0.25
OGGM	Rosalp	82	174	0.27	0.3
CABF	LDG	75	2	0.55	0.6
HINF	LDG	219	18	0.5	0.5
BSF	LDG	217	15	0.45	u
HAU	LDG	230	5	0.45	0.5
LOR	LDG	226	310	0.6	u
VIVF	LDG	160	221	u	0.25
TCF	LDG	302	276	0.6	u
ORIF	LDG	114	185	u	0.3
LPL	LDG	69	133	0.2	0.2
LPG	LDG	71	134	0.2	0.2
MBDF	LDG	143	161	u	0.15–0.2
CALF	TGRS	350	124	0.2	u
OBS	IPSN	226	187	0.3	0.3
RSL	Sismalp	50	124	0.2	0.2
LOMF	Renass	167	20	0.45	0.45

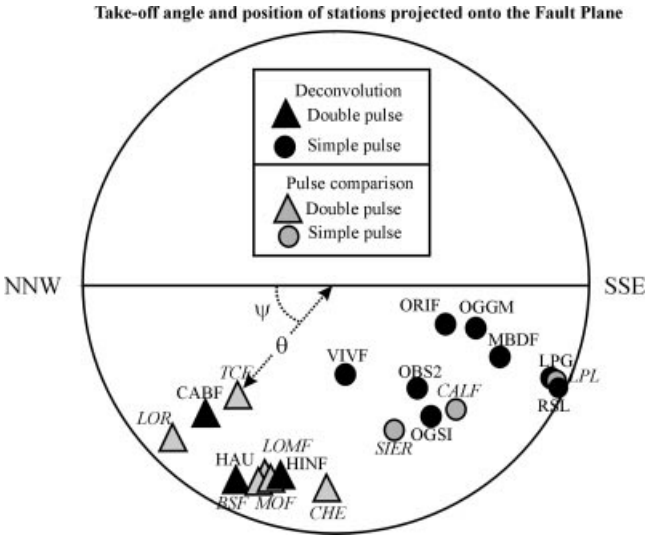

Figure 5. The observed *P* displacement pulses and apparent source-time functions in an equal-area stereographic projection onto the focal sphere viewed along the normal to the fault plane. θ_i is the angle between the ray and the fault normal. ψ_i, measured in the plane of the fault, is the angle between the ray and the strike of the fault.

projected each observation onto the fault plane (Fig. 5). The azimuth and take-off angles of the rays to each station were converted to the angles between the rays and the normal to the fault, θ_i, at the ith station, and between the rays and the strike of the fault, ψ_i, for a fault with strike, dip and rake of 316°, 70° and −10° derived by Thouvenot *et al.* (1998). The take-off angles were calculated for a focal depth of 2 km based on the velocity model used by Thouvenot *et al.* (1998). Since the source is located in the sedimentary layers close to the boundary to the crystalline basement and because of the strong velocity increase across this boundary, all first arrivals beyond an epicentral distance of about 20 km leave the source as down-going rays. Therefore, all our data points come to lie in the lower half of the fault plane. Fig. 5 shows that the projections of the double- and single-pulse source-time functions onto the fault plane separate into two distinct groups. For a unilaterally propagating rupture on a circular fault, the duration of the apparent moment-rate function at the ith station, τ_i, is given by

$$\tau_i = L[1/V_r - 1/c \sin\theta_i \cos(\psi_r - \psi_i)], \quad (1)$$

with L the source diameter, V_r the rupture velocity, c the phase velocity, θ_i the angle between the ray and the normal to the

fault, ψ_i the angle between the ray and the strike of the fault, and ψ_r the direction of rupture propagation (Boatwright 1980). Both ψ_i and ψ_r are measured in the plane of the fault. For given values of τ_i, θ_i and ψ_i and fixed values of c and V_r, we can solve eq. (1) for L as a function of ψ_r. In practice, this gives a different value of L for each observation τ_i.

Increasing ψ_i in steps of 5° over the range between 0° and 360°, we calculate an average value of L over all stations for each value of ψ_r, and search for that ψ_r which minimizes the sum of the squared differences between the observed and calculated τ_i. With reference to Fig. 5 and to the given orientation of the fault plane, $\psi_r = 0°$ or 180° corresponds to a purely horizontal rupture propagation towards the NW (0°) or SE (180°), whereas $\psi_r = 90°$ or 270° corresponds to a purely downward (90°) or upward (270°) rupture direction. Assuming a P-wave velocity of 5.35 km s^{-1} (Thouvenot *et al.* 1998) and an average rupture velocity of 2.7 km s^{-1}, we obtain $\psi_r = 180°$ and $L = 915$ m. The fit between observed and calculated τ_i is better for the single-pulse STFs at the stations with $\psi_i > 120°$, situated in the southeast quadrant relative to the epicentre, than for the double-pulse STFs observed at the stations to the north (Fig. 6). To judge whether the assumption of a unilateral rupture propagation is justified and assess to what extent the rupture direction can be constrained by the available data, we have calculated the mean of the misfit (the squared differences between the observed and calculated τ_i) for every 5° increment in ψ_r. From the resulting plot in Fig. 7, we see that this misfit function has a broad minimum over the range $130° < \psi_r < 250°$. Thus, due to the fact that all our observations correspond to downgoing rays, which span a range of ψ_i of only 120°, the vertical component of the rupture direction is poorly constrained.

It can be argued that, because of the contribution of the small event's STF to the EGF, the deconvolution procedure underestimates the true duration of the STF of the main shock. Considering the magnitude of the EGF events that we used, this deficit could amount to about 0.1 s. As shown by the corresponding misfit function in Fig. 7, adding 0.1 s to all our estimates of τ_i does not change the resulting rupture direction significantly. Similarly, using a different average rupture velocity raises the overall misfit by only a small amount and does not affect the location and breadth of its minimum in a significant way (Fig. 7).

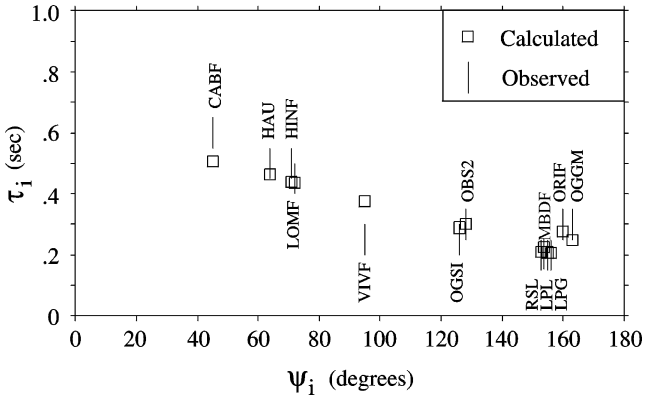

Figure 6. Observed (vertical bars equal to uncertainties) and calculated (squares) values of τ_i as a function of ψ_i.

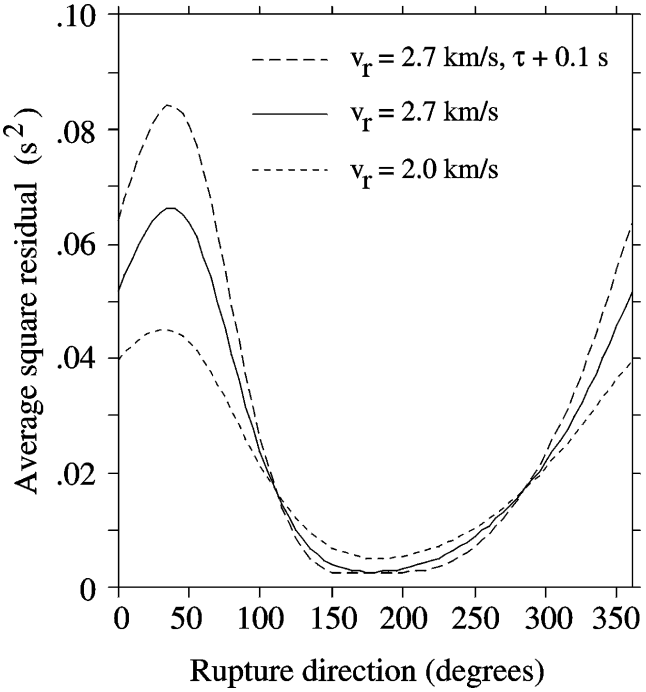

Figure 7. The rms of the differences between the observed and calculated τ_i as a function of ψ_i for various rupture velocities V_r and for τ_i increased by 0.1 s (see text for further explanations).

Subevent location

Based on the values of the ARSTF reported in Table 1, it is possible to estimate the maximum area that was activated during the main shock rupture by constructing the isochrons over the fault (Bernard & Madariaga 1984; Spudich & Frazer 1984; Zollo & Bernard 1991). Starting from the nucleation point (S0 in Fig. 8), the rupture propagates circularly with a constant rupture velocity, and slip is assumed to have a step-like shape in time. An isochron is defined as the locus of all points on the fault from which seismic radiation reaches a given station at a given time t,

$$t = T_R(r_0, r_1) + T_C(r_0, x), \tag{2}$$

where r_0 and r_1 are the nucleation point and the isochron point, and x denotes the receiver position. T_R represents the rupture time, while T_C is the wave propagation time (the P-wave velocity is set to 5.35 km s^{-1} in the medium around the source). We drew the isochrons that delimit the final extension of the rupture for each station. The intersection of the areas delimited by isochrons defines the region of the fault plane that must contain the rupture. This area depends on the rupture velocity. In order to estimate the maximum area of the fault we chose a velocity of 3 km s^{-1}, which can be considered as an upper bound in the sedimentary layer that contains the source.

Fig. 8 shows the isochrons that correspond to six stations distributed over a representative set of azimuths. The intersection of the areas delimited by isochrons gives an estimate of the dimensions of the active fault plane. The grey zone in Fig. 8 represents the rectangular fault that corresponds most closely to the intersection of the areas delimited by the isochrons. Since the rupture velocity that we used is high (3 km s^{-1}), this area, estimated at 2.5 km^2, gives an upper

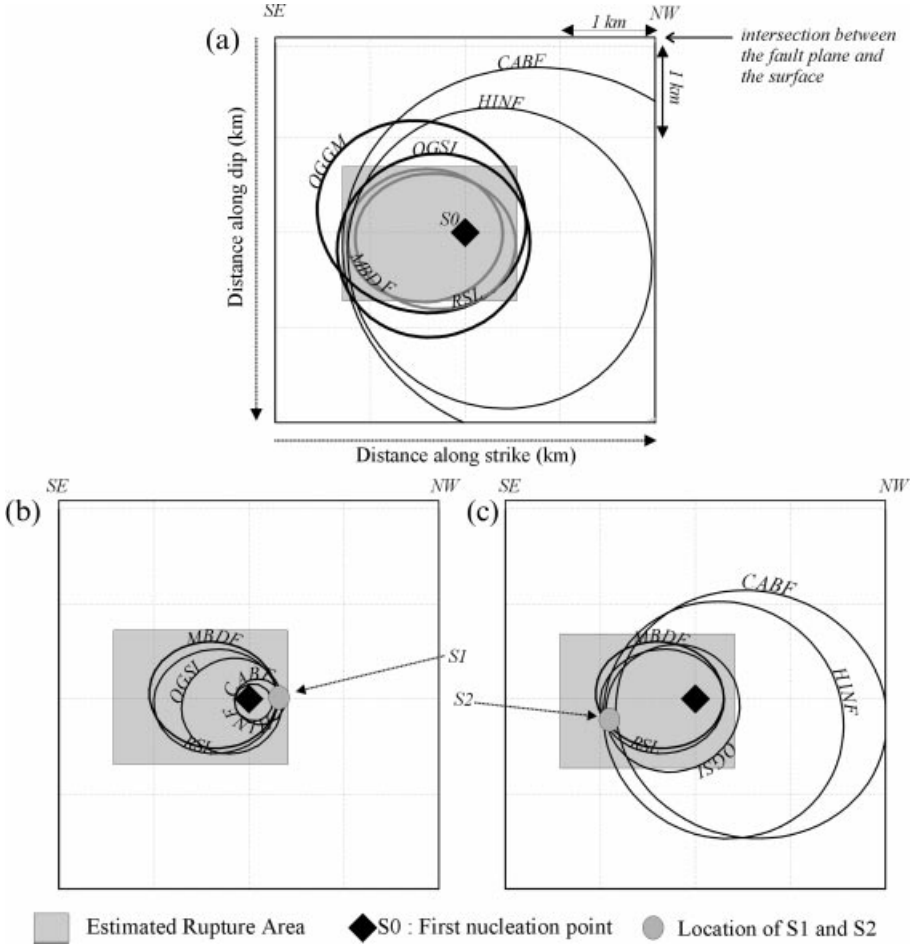

Figure 8. (a) Isochrons corresponding to the total duration of the apparent relative source-time functions represented on the fault plane (the origin of the depth scale along the fault corresponds to the surface). (b) Isochrons corresponding to the peak of the first subevent. (c) Isochrons corresponding to the peak of the second subevent.

bound to the rupture dimension. With the seismic moment equal to 1.9×10^{16} N m (computed from records of a Swiss accelerometer, located 30 km from the epicentre), we obtained an average displacement of 30 cm and a stress drop of 5.5 MPa.

Having obtained an estimate of the total rupture area, we can now locate the two subevents on the fault plane. For this purpose, on the ARSTFs of Fig. 3 we measure the time between the beginning of the rupture and the peak of each subevent. The first subevent, S1, can be seen at every station, whereas S2 is separated clearly from S1 only at the three stations CABF, HAU and HINF to the north and less clearly at station OGSI to the east. At the stations south and southeast of the epicentre, such as MBDF and RSL, the overall rupture directivity has caused the signals of the two subevents to merge into a single pulse. For these two stations we have taken the time from onset to the peak of the ARSTF (the rise time) as representative of both subevents. The isochrons corresponding to the delays of S1 and S2 determined in this manner are shown in the lower part of Fig. 8. The only region where the isochrons of S1 intersect is located about 250 m northwest of the nucleation point, whereas the second subevent, S2, is located about 900 m to the southeast.

It is important to remember that the absolute locations of the subevents depend strongly on the rupture velocity, which could not only be different from the one chosen for our model, but could also vary over the duration of faulting (e.g. Deichmann 1997). However, the general picture would remain the same, with a first subevent close to the hypocentre towards the northwest and a second subevent further away towards the southeast. The fact that the first subevent is located towards the northwest agrees with the interpretation of pulse-width measurements performed on the clipped data, which are based on the first pulse alone.

RELATION TO THE AFTERSHOCKS

The aftershock locations determined by Thouvenot *et al.* (1998), based on data from a temporary seismic network installed in the epicentral area two days after the main shock, delineate two fault segments separated by a right-lateral step-over of about 500 m. The larger segment, with the higher seismic activity in terms of both the number and the size of the events, is to the north and somewhat displaced from the surface trace of the Vuache Fault, while the other is more to the south and closer to the fault trace. Although Thouvenot *et al.* (1998) made an effort to constrain the main shock location with the results of the aftershock measurements and place its epicentre at the southeastern end of the northern fault segment, the remaining location uncertainty can not exclude it from having occurred on the southern segment instead.

Given this uncertainty, Fig. 9 illustrates two end-member scenarios of possible locations of the main shock rupture area relative to the aftershocks: in the first case, the rupture of the main shock nucleated close to the southeastern end of the northern segment and propagated mainly away from the more active part of the aftershock zone, while in the second case it nucleated and propagated along the southern segment. As noted above, the size of the main shock rupture area in Fig. 9 must be regarded as an upper bound.

DISCUSSION AND CONCLUSIONS

The aim of this study was to retrieve the main characteristics of the rupture process of the Epagny–Annecy earthquake using all the available data.

The analysis of the raw *P*-wave displacement seismograms and the EGF deconvolutions show that the rupture process consisted of at least two subevents. Moreover, the azimuthal dependence of the durations of the apparent source-time functions obtained from the EGF deconvolution as well as the fact that the double pulse is visible only on stations north of the epicentre provide evidence for a strong unilateral component of the rupture propagation towards the southeast along the strike of the fault and roughly parallel to the direction of slip. The isochron analysis indicates that a small amount of rupture propagation towards the northwest occurred during the early stages of the rupture process, corresponding to the first subevent, and that the second subevent corresponds to the main part of the rupture, which propagated towards the southeast.

In an attempt to interpret these results in terms of the fault geometry derived from the trend of the Vuache Fault, from the focal mechanism of the main shock and from the aftershock distribution documented by Thouvenot *et al.* (1998), we consider three scenarios: (1) the rupture area of the main shock is entirely part of the northern fault segment; (2) it is entirely part of the southern segment; or (3) the rupture nucleated on the northern segment, producing the first subevent, and then jumped to the southern segment, where it continued to propagate towards the southeast. Because of our lack of unclipped near-source seismograms for the main shock and the limited coverage of the focal sphere of the available data, our results on their own do not allow us to distinguish between these three possibilities. Nevertheless, we can examine the implications of these different scenarios in the light of other observations and arguments.

In the first case, the main shock did not occur on the Vuache Fault but on a fault segment parallel to it. For some not immediately apparent reason, the rupture stopped propagating towards the northwest, and then the main rupture phase propagated away from the area featuring the highest aftershock activity into a region with very few aftershocks. Fletcher & Spudich (1998) observed an apparent lack of correlation between rupture directivity and concentration of aftershock activity in their analysis of three moderate earthquakes on the San Andreas Fault. Therefore, this somewhat counterintuitive behaviour is not a sufficient reason to exclude this scenario. In the second case, the main shock actually nucleated on the Vuache Fault but was prevented from propagating further to the northwest by the apparent stepover in the fault and was thus forced to propagate mainly towards the southeast, as documented by the second subevent. In this scenario, the first subevent would correspond to a stopping phase originating from the northwestern edge of the rupture area, in agreement with the fact that it is observed as a separate phase only in a sector north of the epicentre. The third scenario, which invokes

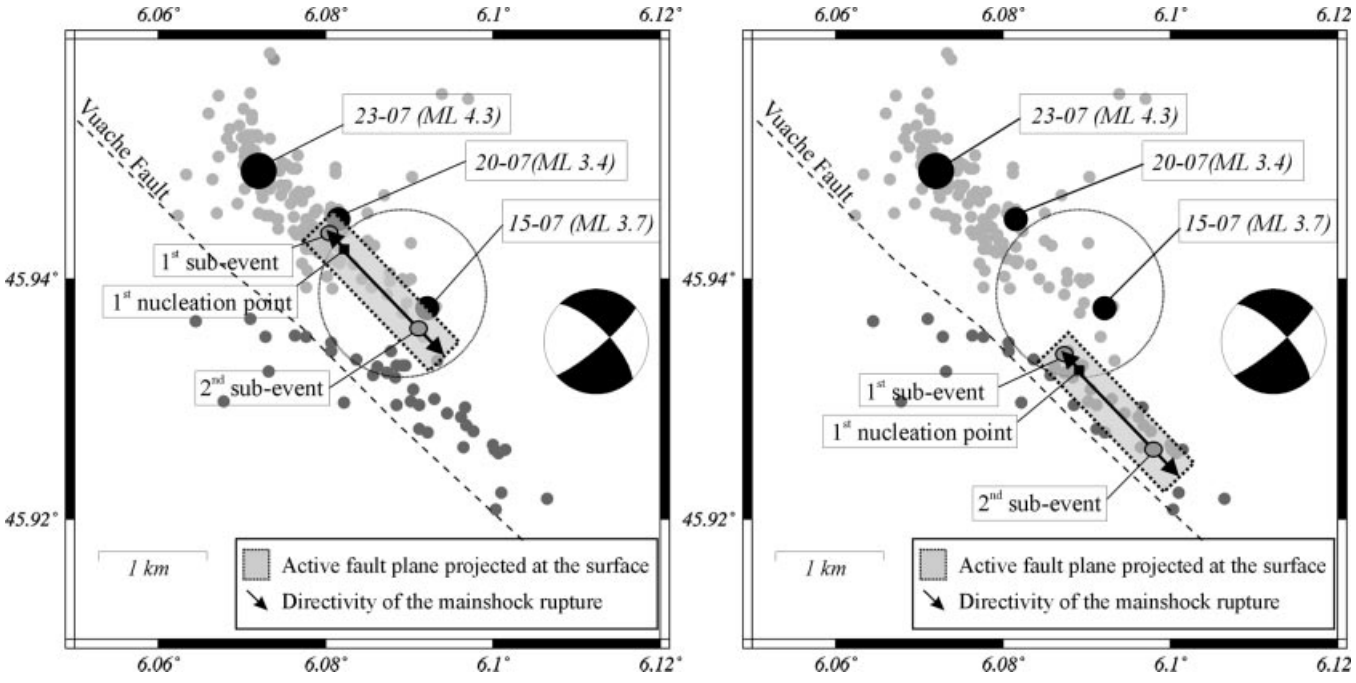

Figure 9. Aftershock locations and focal mechanism from Thouvenot *et al.* (1998). The largest aftershocks are labelled and the circle shows the estimated uncertainty of the main shock's epicentral location. A projection of the fault plane obtained from the isochron analysis is represented by a grey rectangle on which are shown the estimated locations of the first and second subevents as well as the rupture directivity. The two diagrams show the location of the main shock rupture assuming it is part of either the northern (left) or southern fault segment (right).

a rupture process occurring on two separate fault segments, is appealing, because it gives an intuitively plausible explanation for the observation of two subevents. A similar behaviour, with a rupture front that jumps across a stepover from one fault segment to the next, was observed in the 1992 Landers earthquake (Wald & Heaton 1994). However, as in the first scenario, we have to ask why the rupture did not continue further to the northwest, along a segment which, judging from the enhanced aftershock activity, was obviously ready to slip.

In addition to the arguments mentioned above, we favour the second scenario, in which the entire main shock rupture occurred on the southern fault segment and thus on the Vuache Fault, for the following reasons. The estimated total rupture area is compatible with the aftershock distribution on the southern segment. The fact that the number and magnitudes of the southern aftershocks are considerably smaller than those of the northern ones is evidence that most of the stress had already been released by the main shock. Conversely, the stepover in the fault, which prevented the rupture from propagating further to the northwest, then led to a stress increase on the northern segment. This stress increase was then released over the subsequent days and weeks with a large number of aftershocks, including several events of magnitude 3 and 4. Moreover, important evidence in favour of the main shock having occurred on the southern segment is the observation of cracks in the ground and in the runway of the Meythet–Annecy airport exactly where the extrapolated fault plane of the southern fault segment intersects the ground surface (Thouvenot *et al.* 1998). These cracks certainly did not occur as a consequence of the aftershocks alone.

Whatever interpretation one favours, our analysis of the rupture process of the Epagny–Annecy earthquake clearly shows that even moderate events of magnitude 5 can have complex rupture histories. It is also clear that, in addition to the known local site effects, the strong directivity effects due to an asymmetric rupture propagation can have significant consequences for the damage potential of such earthquakes.

ACKNOWLEDGMENTS

We thank the various groups that helped us retrieve the data necessary for this work and especially Marc Nicolas from LDG. We are grateful to François Thouvenot for providing us with the aftershock locations and focal mechanisms as well as for several helpful discussions. This work has been funded by the European project ENV4-CT96–0296 and the IPSN. (Publication no. 237 of UMR Géosciences AZUR and no. 1073 of the Institute of Geophysics, ETH-Zürich.)

REFERENCES

Bernard, P. & Madariaga, R., 1984. A new asymptotic method for the modelling of near-field accelerograms, *Bull. seism. Soc. Am.,* **74,** 539–557.

Beroza, G.C. & Ellsworth, W.L., 1996. Properties of the seismic nucleation phase, *Tectonophysics,* **261,** 209–227.

Boatwright, J., 1980. Spectral theory for circular seismic sources: simple estimates of source dimension, dynamic stress drop and radiated energy, *Bull. seism. Soc. Am.,* **70,** 1–28.

Courboulex, F., Virieux, J., Deschamps, A., Gibert, D. & Zollo, A., 1996. Source investigation of a small event using empirical Green's functions and simulated annealing, *Geophys. J. Int.,* **125,** 768–780.

Courboulex, F., Deschamps, A., Cattaneo, M., Costi, F., Deverchère, J., Virieux, J., Augliera, P., Lanza, V. & Spallarossa, D., 1998. Source study and tectonic implications of the April 21, 1995 Ventimiglia (border of Italy and France) earthquake ($M_L = 4.7$), *Tectonophysics,* **290,** 245–257.

Deichmann, N., 1997. Far field pulse shapes from circular sources with variable rupture velocities, *Bull. seism. Soc. Am.,* **87,** 1288–1296.

Fletcher, J. & Spudich, P., 1998. Rupture characteristics of the three M 4.7 (1992–94) Parkfield earthquakes, *J. geophys. Res.,* **103,** 835–854.

Frankel, A. & Kanamori, H., 1983. Determination of rupture duration and stress drop for earthquakes in southern California, *Bull. seism. Soc. Am.,* **73,** 1527–1551.

Haddon, R. & Adams, J., 1997. Anatomy of a small intraplate earthquake: a dissection of its rupture characteristics using regional data, *Geophys. J. Int.,* **129,** 235–251.

Hartzell, S., 1978. Earthquakes aftershocks as Green's functions, *Geophys. Res. Lett.,* **5,** 1–4.

Hough, S.E., 1996. Observational constraints on earthquake source scaling: Understanding the limits in resolution, *Tectonophysics,* **261,** 83–95.

Lambert, J. & Levret-Albaret, A., 1996. *Mille Ans de Séismes en France, Catalogue d'épicentres, Paramètres et Références,* Ouest Editions, Nantes.

Mori, J., 1996. Rupture directivity and slip distribution of the M 4.3 foreshock to the 1992 Joshua Tree earthquake, Southern California, *Bull. seism. Soc. Am.,* **86,** 805–810.

Mueller, C., 1985. Source pulse enhancement by deconvolution of an empirical Green's function, *Geophys. Res. Lett.,* **12,** 33–36.

Nicolas, M., Santoire, J.P. & Delpech, P.Y., 1990. Intraplate seismicity new seismotectonic data in western Europe, *Tectonophysics,* **179,** 27–53.

O'Neill, M.E. & Healy, J.H., 1973. Determination of source parameters from P-wave rise time, *Bull. seism. Soc. Am.,* **63,** 599–614.

Spudich, P. & Frazer, L.N., 1984. Use of ray theory to calculate high frequency radiation from earthquake sources having spatially variable rupture velocity and stress drop, *Bull. seism. Soc. Am.,* **74,** 2061–2082.

Thouvenot, F., Fréchet, J., Tapponnier, P., Thomas, J.C., Le Brun, B., Ménard, G., Lacassin, R., Jenatton, L., Grasso, J.R., Coutant, O., Paul, A. & Hatzfeld, D., 1998. The M_L 5.3 Epagny (French Alps) earthquake of 15 July 1996: a long-awaited event on the Vuache fault, *Geophys. J. Int,* **135,** 876–892.

Vogt, J., ed., 1979. Les tremblements de Terre en France, *Mém. Bur. Rech. géol. min.,* no. 96.

Wald, D.J. & Heaton, T.H., 1994. Spatial and temporal distribution of slip for the 1992 Landers, California, earthquake, *Bull. seism. Soc. Am.,* **84,** 668–691.

Zollo, A. & Bernard, P., 1991. How does an asperity break? New elements from the waveform inversion of accelerograms for the 2319 UT, October 15, 1979, Imperial Valley aftershock, *J. geophys. Res.,* **96,** 549–573.